ENVIRONMENTAL RESEARCH
LETTERS

LETTER • OPEN ACCESS

Modulation of dense shelf water salinity variability in the western Ross Sea associated with the Amundsen Sea Low

ENVIRONMENTAL RESEARCH
LETTERS

LETTER

Modulation of dense shelf water salinity variability in the western Ross Sea associated with the Amundsen Sea Low

Guijun Guo[1,2], **Libao Gao**[1,2] and **Jiuxin Shi**[2,3]

[1] Center for Ocean and Climate Research, First Institute of Oceanography, Qingdao, People's Republic of China
[2] Qingdao National Laboratory for Marine Science and Technology, Qingdao, People's Republic of China
[3] Physical Oceanography Laboratory, Ocean University of China, Qingdao, People's Republic of China

E-mail: guoguijun@fio.org.cn and gaolb@fio.org.cn

Keywords: dense shelf water, freshwater input, large-scale circulation, Ross Sea, Amundsen Sea low

Supplementary material for this article is available online

OPEN ACCESS

RECEIVED
12 June 2020

REVISED
25 September 2020

ACCEPTED FOR PUBLICATION
11 November 2020

PUBLISHED
18 December 2020

Abstract

Dense shelf water (DSW) produced in the western Ross Sea (RS) is one of the major sources of Antarctic bottom water (AABW). Thus the understanding of long-term variability of DSW salinity and its controlling factors in the western RS is critical to assess the variability of globally distributed AABW. Here we analyze a long time record of hydrographic data (1984–2020) collected in the western RS, as well as sea ice drift vectors, surface wind speed, sea level pressure and Amundsen Sea low (ASL) indices. We confirm recent findings that there is a rapid increase of DSW salinity in the western RS after a minimum in 2013, although the DSW has experienced substantial freshening in the past few decades, indicating a significant multidecadal variability of DSW salinity in the western RS. Over the past four decades, multidecadal variability in the DSW salinity has been strongly coupled with westward zonal flow changes along the coastal current, and the post-2013 rapid enhancement of DSW salinity is accompanied by reduced freshwater input due to weakening of the westward zonal flow from the upstream Amundsen Sea (AS) into the RS. Large-scale circulation determining the strength of the zonal flow is closely linked to the ASL variability. The accelerated deepening of the ASL and the resulting southwestward extension of low pressure induce an eastward coastal current anomaly. This reduces the freshwater input from the AS to the RS and is responsible for the subsequent enhancement of DSW salinity in recent years in the western RS. These dynamical processes demonstrated here explain how the ASL changes modulate the DSW salinity in the western RS, and will help to understand the implication of climate changes in the Southern Ocean on AABW formation.

1. Introduction

The Southern Ocean is considered to be sensitive to climate changes and is warming more quickly than lower latitudes (Böning *et al* 2008, Gille 2008, Gao *et al* 2018). This rapid warming is ascribed to the remarkable strengthening of the circumpolar westerlies, which is thought to increase the upwelling rate (Le Quéré *et al* 2007, Meredith *et al* 2012) of warm circumpolar deep water (CDW), as well as the transport of CDW onto the Antarctic continental shelves (Thoma *et al* 2008, Dinniman *et al* 2012, Spence *et al* 2014). This increase in oceanic heat over the shelf brought by CDW intrusion drives an increasing basal melt rate of the ice shelves and increases the freshwater input to shelf regions (Pritchard *et al* 2012, Rignot *et al* 2013, Paolo *et al* 2015, Rintoul *et al* 2016, Adusumilli *et al* 2020), which in turn reduces the density of dense shelf water (DSW), suppresses Antarctic bottom water (AABW) formation (Williams *et al* 2016) and has a profound implication for global thermohaline circulation (Lumpkin and Speer 2007, Marshall and Speer 2012).

The Ross Sea (RS, figure 1(a)), the largest embayment of the Southern Ocean around Antarctica, provides the densest DSW on the continental shelf resulting from the vigorous release of brine through sea ice production during autumn and winter (Jacobs *et al* 1970, Orsi and Wiederwohl 2009). This

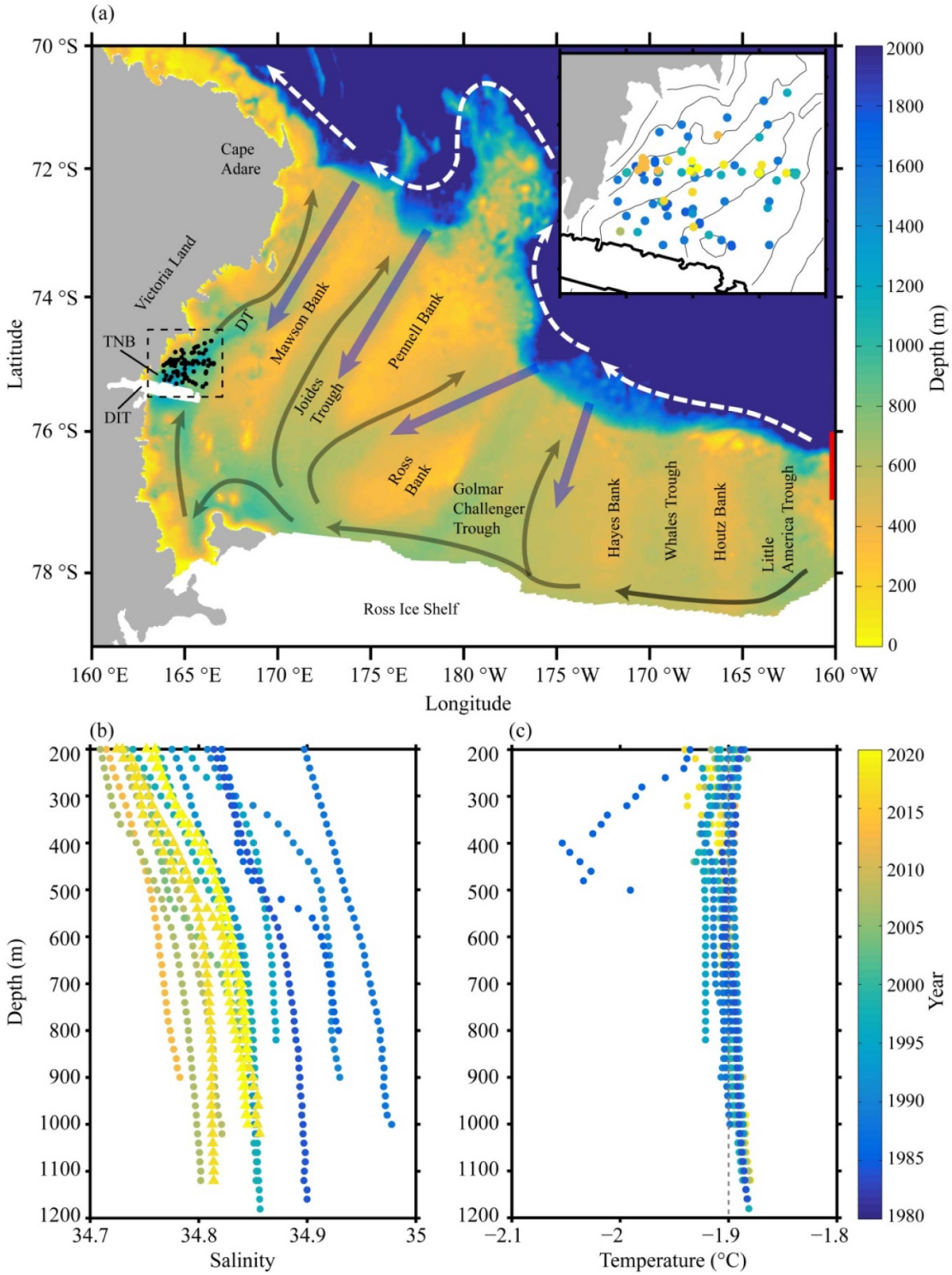

Figure 1. (a) Map of the Ross Sea and the observational stations in the Terra Nova Bay polynya (TNBP, dashed box). The inset zooms into the TNBP stations, with sampling years color coded the same as in (b) and (c). White dashed and gray lines in (a), respectively, represent the general currents along the shelf break and on the shelf, and thick blue arrows indicate the paths of CDW intrusion onto the shelf (referred to Budillon *et al* (2003), Smith *et al* (2014)). The thick red line represents the section at the AS/RS gate for zonal flow estimates. (b) and (c), Annual mean profiles of salinity and temperature, color coded by sampling years. Salinity profiles increased rapidly after 2013 are highlighted by triangles. Surface freezing temperature (−1.9 °C) is shown as a vertical dashed line in (c). Topographical features in (a) are: TNB = Terra Nova Bay; DIT = Drygalski Ice Tongue; DT = Drygalski Trough.

makes the RS an optimal site for AABW formation and export to the global ocean (Orsi *et al* 1999, Gordon *et al* 2009, 2015), contributing ∼25% of all AABW formation on Antarctic shelves (Orsi *et al* 2002). DSW outflows in the RS occur at the Drygalski Tough and the Glomar-Challenger Trough, where the DSW is dominated by high salinity shelf water and ice shelf water respectively. High salinity

shelf water in the northern Drygalski Trough has freshened by ∼0.06 between 1995 and 2006, while the ice shelf water in the northern Glomar-Challenger Trough has freshened by ∼0.04 during 1998–2006 (Budillon *et al* 2011). Changes of these thermohaline characteristics in the RS linked to AABW formation will likely have substantial impacts at the global scale by impacting thermohaline circulation (Johnson 2008, Orsi and Wiederwohl 2009, Jacobs and Giulivi 2010).

The ocean circulation on the RS continental shelf consists of two main inflows from the east, the Antarctic Coastal Current and Antarctic Slope Current (figure 1(a)) (Budillon *et al* 2003, Smith *et al* 2014), which are driven by easterly wind along the coast. The westward inflows are critical to carry freshwater from the upstream Amundsen Sea (AS) into the RS, contributing to the long-term variability of DSW salinity in the RS (Jacobs and Giulivi 2010, Nakayama *et al* 2014). In the past few decades, ocean measurements in the RS have revealed marked decreases (∼0.03 decade^{-1}) in the salinity of DSW (Jacobs *et al* 2002, Jacobs and Giulivi 2010). However, beginning in 2014 the DSW salinity in the RS has rapidly increased (Castagno *et al* 2019). In addition to changes in the freshwater inflow from upstream, several other mechanisms are also potentially responsible for the variability of DSW salinity, such as sea ice production in coastal polynyas, Ross Ice Shelf melting, changes in CDW intrusion onto the shelf region and precipitation (Jacobs *et al* 2002, Castagno *et al* 2019).

Sea ice production in Terra Nova Bay polynya (TNBP) and RS polynya (RSP) shows little change with time (Tamura *et al* 2016), and is believed to govern the DSW salinity only within the seasonal cycle (Assmann and Timmermann 2005). Changes in CDW intrusion onto shelf (Castagno *et al* 2017, 2019), precipitation and Ross Ice Shelf melting (Jacobs *et al* 2002, Jacobs and Giulivi 2010) are also believed to have little impact on DSW salinity. Basal melt rates of ice shelves in West Antarctica have large interannual and decadal variability (Paolo *et al* 2018, Adusumilli *et al* 2020). During 1994–2018, meltwater fluxes from basal melt of ice shelves in the AS sector increase to a maximum in 2009 and then decline incrementally to near steady-state values after that (Adusumilli *et al* 2020). However, mass loss of ice sheet in West Antarctica has increased from 1979 to 2017 (Shepherd *et al* 2018, Rignot *et al* 2019), indicating an increasing freshwater flux into the ocean via basal melt of ice shelves as well as iceberg calving (Depoorter *et al* 2013). This would decrease rather than increase the salinity of DSW in the western RS after 2014 (Castagno *et al* 2019). Therefore, long-term freshening of DSW in the RS is ascribed to increased freshwater transport from the upstream AS in earlier studies (Jacobs and Giulivi 2010, Budillon *et al* 2011), and the rapid increase of DSW salinity since 2014 is also related to large-scale forcing that reduces the freshwater input to the RS (Castagno *et al* 2019). The westward coastal current is critical to freshwater inflow to the RS (Nakayama *et al* 2014). However, in the presence of sea ice in Antarctic regions, satellite altimetry cannot measure SSH well enough to get geostrophic currents, hence the exact mechanism linking the DSW salinity variability to large-scale circulation and climate phenomena remains largely uncertain.

Several studies have documented the possible link between the advection of low-salinity water from increased mass loss of ice sheets upstream and the long-term freshening of the RS (Nakayama *et al* 2014, Smith *et al* 2014, Dinniman *et al* 2018). In contrast, Assmann and Timmermann (2005) argue that the steady decrease in DSW salinity reported by Jacobs *et al* (2002) is an aliasing artifact due to irregular sampling and deduce a multidecadal oscillation in DSW salinity superimposed on the long-term freshening trend from model results. The long time series of DSW salinity in Jacobs *et al* (2002) and Assmann and Timmermann (2005) are derived from the RSP north of Ross Island, which is one of the most densely sampled regions at that time. However, the DSW formed in the RSP ($S < 34.76$) is less saline than that formed in the TNBP ($S > 34.8$) (Orsi and Wiederwohl 2009), and changes in the DSW of the TNBP are believed to have greater effects on AABW formation than that of the RSP (Jendersie *et al* 2018). Thus, understanding the long-term changes in DSW in the TNBP and their governing factors is critical to assess AABW changes in Antarctic region.

A substantial component of interannual atmospheric variability in the Pacific Sector of Antarctica, as a potential driver of ocean variability, is associated with the AS low (ASL) (Turner *et al* 2017, Raphael *et al* 2019). The ASL is a highly dynamic and mobile climatological low pressure system located in the Pacific Sector of the Southern Ocean (Hosking *et al* 2013).The intensity and location of the ASL play a key role in modulating the zonal and meridional winds between the Antarctic Peninsula and the RS (Turner *et al* 2017, Paolo *et al* 2018, Raphael *et al* 2019), thus the wind-driven circulation and horizontal transport in this region are also expected to be related to the ASL changes. Here we used the hydrographic datasets collected in the TNBP over the past four decades, as well as the available sea ice drift vectors, surface wind speed, sea level pressure (SLP) and the ASL indices, to investigate how the ASL changes modulate DSW salinity in the western RS through affecting large-scale circulation. In particular, we investigated the response of westward zonal current on the shelf to the ASL changes, which determines the freshwater input from the upstream AS into the RS, to provide new insight into the impacts of climate changes on DSW production which is critical to AABW formation.

2. Data and methods

2.1. Hydrographic data

The temperature and salinity profiles collected in the TNBP during 17 years within the period of 1984–2020 were used in this study (figure 1). Profiles of years before 2013 were obtained from the World Ocean Database (WOD13, table S1 (available online at stacks.iop.org/ERL/16/014004/mmedia)) (Boyer *et al* 2013), and only data records with maximum depths larger than 600 m were used. There were also available datasets in 2010 and 2011 in WOD13 collected by instrumented seals, but they were not used in this study due to their relatively low salinity accuracy (∼0.05) (Roquet *et al* 2014). The hydrographic data profiles in and after 2013 were collected by Chinese National Antarctic Research Expedition cruises using a Sea-Bird SBE 911plus conductivity–temperature–depth (CTD) profiler, except for the XCTD deployment in 2018. The XCTD data was validated by a comparison test during the summer cruise in 2020, which showed that the salinity profiles derived from two XCTDs agreed well with that obtained from the SBE 911plus CTD profiler (figure S1(a)) and the salinity differences were generally less than 0.01 (figure S1(b)). To minimize seasonal aliasing, only data from the more heavily sampled summer months (table S1) were used and all the profiles were interpolated to 10 m bins linearly for an easier comparison. This work focused on deep layers below 600 m to eliminate the effects of short-term processes at the surface. The horizontal standard deviation (std) of the salinity among all stations in each year below 600 m were generally less than 0.01 (figure S2), while the std at each layer was set to 0 when only one profile was available in a particular year. The highest std occurred in 1988, in which the observational stations covered the largest area in TNBP (inset map in figure 1(a)), but the averaged std value over the layer below 600 m was still less than 0.01. This is small compared to the scale of the multidecadal variability of DSW salinity (figure 1(b)), indicating that the spatial differences for observational stations are unlikely to alias the results.

2.2. Ocean current calculation

Daily surface wind velocity was used to calculate mean ocean current in the RS by subtracting wind effect from ice motion vectors. The daily sea ice motion data (NSIDC-0116, version 4.1) for 1979–2018 was obtained from the National Snow and Ice Data Center with a resolution of 25 km (Tschudi *et al* 2019). The daily surface wind was derived from the mean values of 10 m wind velocity at 00, 06, 12 and 18 (UTC) in ERA5 reanalysis, which is produced by the European Centre for Medium-Range Weather Forecasts on a high resolution 0.25° × 0.25° (Copernicus Climate Change Service 2017). After mapping the daily ice motion vectors linearly onto the same grid as for the surface wind data, we used a linear relation rule described by Thorndike and Colony (1982) to relate ice motion (u_{ice}, v_{ice}), surface wind velocity (U_{10}, V_{10}) for the same day, speed reduction factor F, turning angle θ, and mean ocean current ($\overline{u_{oc}}$, $\overline{v_{oc}}$).

$$\begin{bmatrix} u_{ice} \\ v_{ice} \end{bmatrix} = F \begin{bmatrix} \cos\theta & -\sin\theta \\ \sin\theta & \cos\theta \end{bmatrix} \begin{bmatrix} U_{10} \\ V_{10} \end{bmatrix} + \begin{bmatrix} \overline{u_{oc}} \\ \overline{v_{oc}} \end{bmatrix}.$$

Following the forms shown by Kimura and Wakatsuchi (2000) and Kimura (2004), the speed reduction factor F, and turning angle θ, were calculated by using a least squares technique as:

$$\theta = \arctan\left[\frac{\sum U'_{10}v'_{ice} - \sum V'_{10}u'_{ice}}{\sum U'_{10}u'_{ice} + \sum V'_{10}v'_{ice}}\right],$$

$$F = \frac{c_1 + c_2 - c_3 + c_4}{\sum U'^2_{10} + \sum V'^2_{10}},$$

where

$$c_1 = \cos\theta \sum U'_{10}u'_{ice},\ c_2 = \sin\theta \sum V'_{10}u'_{ice},$$
$$c_3 = \sin\theta \sum U'_{10}v'_{ice},\ c_4 = \cos\theta \sum V'_{10}v'_{ice},$$

and $\overline{U_{10}}$, $\overline{V_{10}}$, $\overline{u_{ice}}$ and $\overline{v_{ice}}$ are yearly mean values of U_{10}, V_{10}, u_{ice} and v_{ice}. U'_{10}, V'_{10}, u'_{ice} and v'_{ice} are $\left(U_{10} - \overline{U_{10}}\right)$, $\left(V_{10} - \overline{V_{10}}\right)$, $\left(u_{ice} - \overline{u_{ice}}\right)$ and $\left(v_{ice} - \overline{v_{ice}}\right)$, respectively. Generally, thick ice and high ice concentration in the Southern Ocean cause a large ice stress gradient and lower the value of F, hence suppress the ice motion (Steele *et al* 1997, Kimura 2004). With the yearly mean ice motion, surface wind, calculated F and θ, the yearly mean ocean current ($\overline{u_{oc}}$, $\overline{v_{oc}}$) can be calculated as:

$$\begin{bmatrix} \overline{u_{oc}} \\ \overline{v_{oc}} \end{bmatrix} = \begin{bmatrix} \overline{u_{ice}} \\ \overline{v_{ice}} \end{bmatrix} - F \begin{bmatrix} \cos\theta & -\sin\theta \\ \sin\theta & \cos\theta \end{bmatrix} \begin{bmatrix} \overline{U_{10}} \\ \overline{V_{10}} \end{bmatrix}.$$

In this study, only sea ice drift and surface wind data in April–October were used due to rare sea ice coverage on the shelf in other months. The yearly mean ocean current, ($\overline{u_{oc}}$, $\overline{v_{oc}}$), in each year were derived by combining daily ice motion vectors and surface wind velocity in April–October in the corresponding year via the formula above, and time variation of F, θ and ($\overline{u_{oc}}$, $\overline{v_{oc}}$) in each year were assumed to be negligible in this formula (Kimura and Wakatsuchi 2000, Kimura 2004).

The existence of landfast sea ice may lead to large bias in mean ocean current calculation. Nihashi and Ohshima (2015) report that there is little landfast ice along the Ross Ice Shelf calving front due to the occurrence of RSP in winter seasons. Most landfast sea ice occurs west of the RS, but only occupies a narrow region fairly close to the coast. Meanwhile, sea ice motion data close to the Antarctica coast were excluded (figure S3), eliminating the effect of landfast ice on the mean ocean current calculation. Kimura (2004) report that the ocean current derived

using this method in the Southern Ocean is fairly reasonable compared with previous model results, convincing us the reliability of this method used to calculate ocean current. The derived mean ocean current averaged over 1979–2018 in the RS also agrees well with the results presented in Kimura (2004) (figure S3). Based on the yearly mean ocean current in the RS region, the westward zonal flow along the coastal current from the upstream AS to the RS was also examined. This current is critical to the inflow of freshwater from the AS into the RS, which is considered among the main contributors to the long-term freshening in the RS (Jacobs and Giulivi 2010). The calculated surface ocean current was used to estimate barotropic component of zonal flow changes assuming no vertical shear. This barotropic assumption likely overestimates the net transport and variability of the zonal flow because the baroclinic structure is omitted due to the lack of subsurface measurements beneath the ice. However, the barotropic mode is reported to dominate the transport variability of the coastal current in the RS (Dotto *et al* 2018), thus variability of the calculated ocean current here can characterize the actual changes of the current on the shelf to a large extent. Hence the zonal flow was estimated as the mean zonal velocity of the derived ocean current across a section at the AS/RS gate extending from a point (77° S) on the shelf northward to 76° S along 160° W (figure 1(a)). The derived ocean current close to the coast was excluded when doing the zonal flow analysis due to the uncertainty caused by landfast ice.

2.3. Investigation of drivers of circulation changes

The maximum covariance analysis (MCA) (Bretherton *et al* 1992, Wallace *et al* 1992) was used to capture the dominant coupled modes between the yearly mean SLP and the circulation field derived from ice motion vectors and surface wind velocity in the RS during 1979–2018. As the derived ocean current represents mean state of the circulation in a year and the seasonal dependence is not considered (Kimura 2004), the yearly mean SLP was obtained by averaging the SLP data over all months in a year. Then the MCA was achieved by using singular value decomposition of the temporal covariance matrix. The resulting pairs of singular vectors represent the spatial pattern of each field, and the associated temporal coefficients depict the temporal variation in the spatial patterns. Yearly mean SLP was calculated from the ERA5 (Copernicus Climate Change Service 2017), the same reanalysis data as for the daily wind velocity. Then the yearly mean SLP field was analyzed via MCA with the derived yearly mean ocean current. The means and linear trends of both the SLP and ocean current were subtracted before the MCA was performed. The yearly ASL indices (central pressure and location of the ASL) (Hosking *et al* 2016) were also used to evaluate the potential drivers modulating the large-scale circulation and coastal currents on the shelf, which are found to be responsible for salinity changes in the TNBP (Jacobs and Giulivi 2010, Budillon *et al* 2011).

3. Results and discussions

3.1. Multidecadal variability of DSW salinity

Figure 1(b) shows the annual mean profiles of salinity and temperature beneath 200 m collected in the TNBP over the past four decades. The profiles suggest an overall decrease in DSW salinity since the 1980s, with a relatively stable temperature that remains at the surface freezing temperature of −1.9 °C, except for the cold Ice Shelf Water (colder than surface freezing temperature) signal observed in some individual years at 200–500 m. Figure 2(a) shows a time series of the vertical mean salinity of deep layers below 600 m depth in TNBP, represented as a change in the densest DSW in the western RS. The substantial decreasing trend of DSW salinity of deep layers before 2013 is estimated to be 0.052 ± 0.026 decade^{-1} (significant at 99% confidence level), freshening at a higher rate than that estimated by Jacobs *et al* (2002) and Jacobs and Giulivi (2010). However, notably, the freshening trend appears to reverse beginning in about 2013. Although the absolute salinities at all depths after 2013 show lower values than those in the 1980s, there is a rapid increase in the salinity after a minimum in 2013 (figure 1(b)), indicating a recent rebound of DSW salinity in the western RS. To emphasize the multidecadal variability of DSW salinity, we focused on the detrended time series of salinity and its potential drivers, which emphasize the shorter term variability (figure 2).

3.2. Westward zonal flow changes

The rapid enhancement of DSW salinity in recent years is also reported by Castagno *et al* (2019). After evaluating the potential contributors to the long-term variability of DSW salinity (section 1), Castagno *et al* (2019) ascribe the rapid increase of DSW salinity in recent years to large-scale forcing which determines the freshwater input from upstream regions to the RS. However, the exact linkage between large-scale circulation modulated by atmospheric forcing and DSW salinity changes are not resolved because the ocean current is difficult to estimate in Antarctic regions. Here, based on yearly mean ocean current derived from ice motion vectors and surface wind velocity, we extended the studies in Castagno *et al* (2019) and illustrated how the ASL modulates the DSW salinity by affecting large-scale circulation that influences the freshwater input to the RS.

The zonal mean velocity across the AS/RS gate section derived from yearly mean ocean current is presented in figure 2(b). This flow is critical to the spreading of freshwater from the AS westward to the continental shelf of the RS (Nakayama *et al* 2014). The mean zonal flow across the section (figure 1(a))

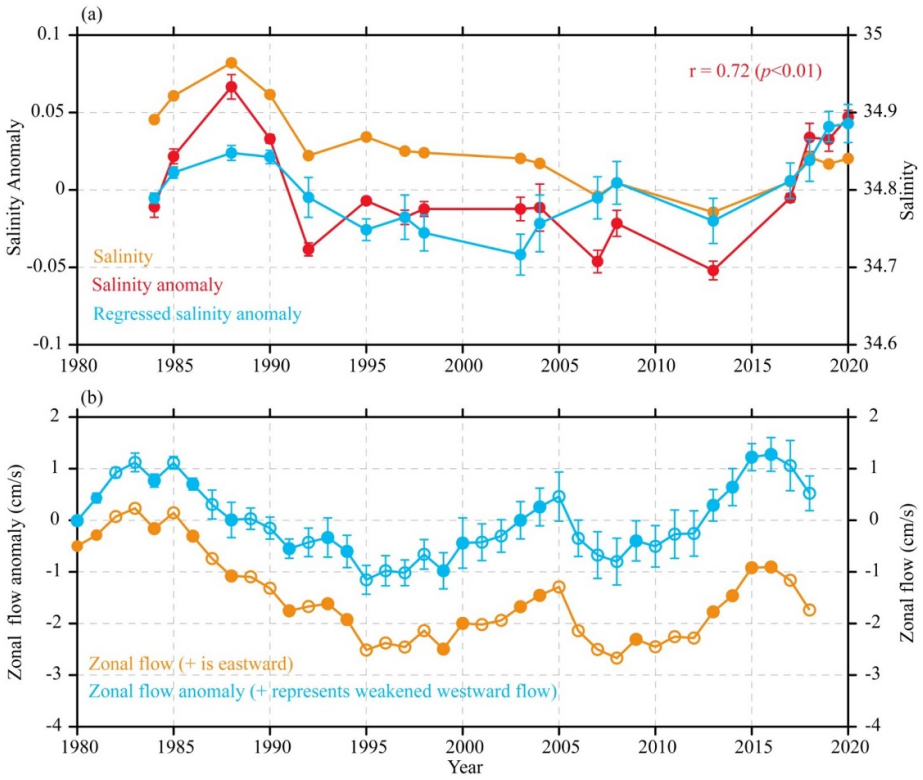

Figure 2. Time series of salinity in TNBP and zonal flow across the section at the AS/RS gate. (a) Annual mean salinity blow 600 m depth. The red line represents detrended salinity (left scale), the blue line represents the regression of detrended salinity onto the detrended zonal flow at the AS/RS gate section 4 years prior (left scale), and the orange line represents the actual salinity (right scale). Correlation coefficient and p value between the detrended salinity and its regressed values are also depicted in (a). (b) Three-year running mean of detrended (blue, left scale) and actual (orange, right scale) zonal flow at the AS/RS gate. Closed circles in (b) represent corresponding data 4 years prior to the salinity records. Vertical standard deviation of the annual mean salinity profiles below 600 m depth in TNBP is overlaid as error bar on detrended salinity in (a). The error bar in (b) is the standard deviation among all grid cells along the gate section, estimated on the derived yearly mean ocean current. Standard deviation of the regressed detrended salinity induced by the ocean current is also overlaid (blue error bar in (a)).

is 1.47 ± 1.01 cm s^{-1}, and exhibits a significant multidecadal variability (figure 2(b)). Time series of the zonal flow anomaly evolve with time similar to the DSW salinity anomaly shown in figure 2(a). The salinity anomaly and their regression onto the zonal flow anomaly 4 years prior are closely correlated at 0.72 ($p < 0.01$). As all the salinity profiles were sampled in summer months (table S1) and deep DSW near the sea bed in TNBP is renewed every year in the austral winter due to strong polynya activity (Rusciano *et al* 2013), DSW salinity from these profiles is expected to represent that of previous year to a large extent. By contrast, the ocean currents are derived as yearly mean values from sea ice motion and surface wind data in April–October. This means that freshwater from the AS flowing across the gate section travels about 3 years before reaching the sampling locations in TNBP, and contributes to local salinity changes. The mean absolute velocity along the coast from the AS/RS gate to the TNBP is estimated to be 1.21 ± 0.24 cm s^{-1}, enabling the water parcel to travel on average 1145 ± 227 km in 3 years after leaving the AS/RS gate, which roughly agrees with the distance from the gate to the TNBP along the coast (∼1200 km). For instance, salinity anomaly regressed onto the zonal flow anomaly 4 years prior increased by 0.039 in 2018 compared to that in 2013, comprised 46% of the salinity anomaly differences between 2018 and 2013. Hence, the multidecadal variability of DSW salinity is strongly modulated by the strength of the westward coastal current, which determines the volume of the freshwater input from the AS to shelf regions of the RS. By this mechanism, the weakened westward coastal current after 2010 (figure 2(b)) reduces freshwater input to the RS, and is responsible for the rapid enhancement of DSW salinity in recent years (figure 2(a)).

3.3. Evolution of large-scale circulation

Multidecadal variability of DSW salinity in the western RS is closely linked to the westward zonal flow along the coastal current (figure 2), which determines the freshwater input from the upstream AS to the RS. The westward coastal current is associated with large-scale circulation in the Ross Gyre (Dotto *et al* 2018) and here the yearly mean ocean current derived from ice motion vectors and surface wind velocity was used to assess long-term variability of large-scale circulation. Variability of large-scale circulation is associated with SLP (Dotto *et al* 2018), which is

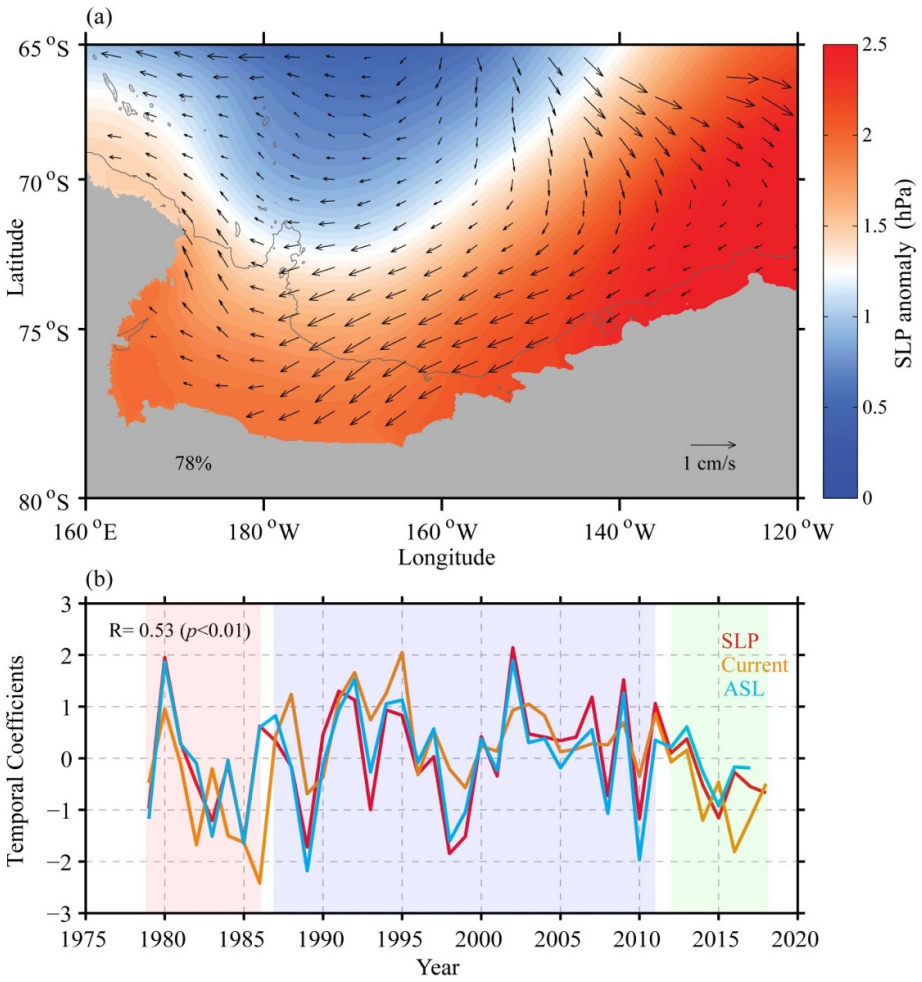

Figure 3. Spatial pattern (a) and associated temporal coefficients (normalized by one standard deviation) (b) of the first MCA mode between the detrended mean ocean current and SLP data over the RS for 1979–2018. The 1000 m isobath is presented by the gray line in (a), and the amplitudes of spatial patterns are scaled by one standard deviation of the corresponding temporal coefficients. The correlation coefficient and p value between the temporal coefficients of the first MCA mode are shown in (b), along with the ASL index, by a blue line normalized by one standard deviation. The detrended ocean current was analyzed only at grids with data available for all studied years. The light shading in (b) indicates different phases dominated by negative/positive values for the normalized temporal coefficients of ocean current mode (orange line).

reported to be modulated to a large extent by the ASL in West Antarctica (Turner *et al* 2013). Here, we applied MCA between the derived mean ocean current and the SLP data over the most recent four decades, 1979–2018, to examine the atmospheric forcing of the multidecadal variability of the circulation and its effects on westward transport of freshwater along coastal current. For the two fields used here, the leading modes of the MCA patterns represent the patterns of SLP anomalies in the RS that most strongly influence the ocean current anomalies and the resulting freshwater transport of the coastal current.

The first leading MCA mode of the coupled ocean current anomaly and SLP anomaly field (figure 3(a)) accounts for 78% of the total squared covariance. The MCA1 patterns display an increased SLP and a westward ocean current anomaly in the ASL domain. The spatial pattern of the ocean current anomaly closely resembles that of the SLP, changing along the isolines of SLP anomalies. The associated temporal coefficients of the first MCA mode between the detrended ocean current and SLP field are significantly correlated ($r = 0.53$ with $p < 0.01$, figure 3(b)), indicating the dominant modulation of the SLP changes in horizontal transport. Figure 2 shows that the multidecadal variability of DSW salinity is modulated by zonal flow variability from the AS with 4 years lag via controlling freshwater input to the RS. Similar to the temporal evolution of the zonal flow at the AS/RS gate, the associated time series of ocean current patterns in figure 3(b) exhibit a dominant negative phase before 1987 (light red shading), followed by a dominant positive phase until 2011 (light blue shading) and a return to the negative phase beginning in 2012 (light green shading). The significantly coupled temporal coefficients obtained from MCA are closely related to the ASL index ($r = 0.93$, $p < 0.01$ and $r = 0.51$, $p < 0.01$ for SLP and ocean current anomaly, respectively) (figure 3(b)). This suggests that the ASL dominates the long-term variability of the freshwater

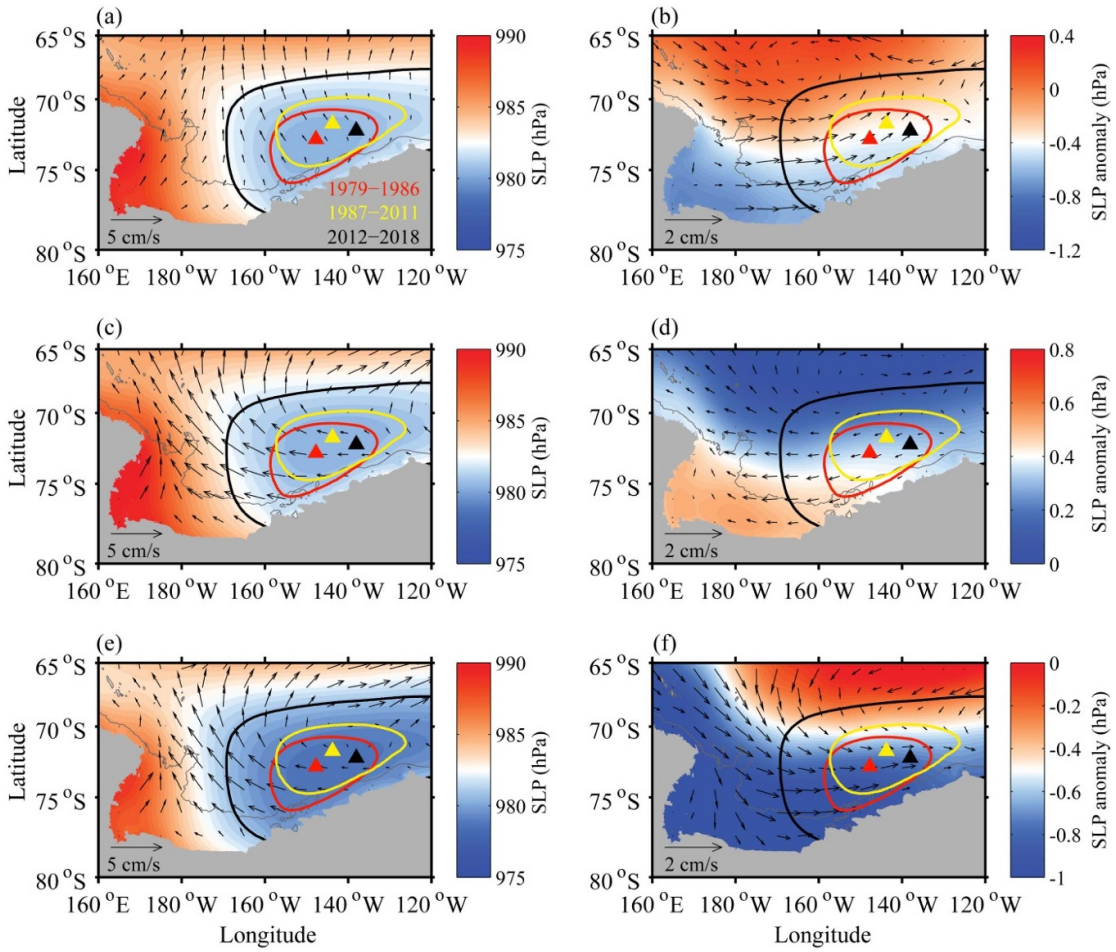

Figure 4. Mean (left panels) and detrended (right panels) patterns of SLP (shading, hPa) and ocean current (vectors) in three phases. (a) and (b), Phase I (averaged over 1979–1986); (c) and (d), Phase II (averaged over 1987–2011); (e) and (f), Phase III (averaged over 2012–2018). Detrended ocean current is calculated only at grids with data available for all studied years. The 1000 m isobath is presented as a gray line. Red, yellow and black contour lines and triangles designate 981 hPa and mean locations of the ASL center in phase I, II, III, respectively.

input from the AS to the RS by affecting the zonal wind at the southern edge of the ASL domain, as reported by Raphael *et al* (2019), which is linked to the barotropic transport of the coastal current.

To study the effect of the variability in the ASL on the large-scale circulation changes and the resulting freshwater input along the coastal current from the AS into the RS, we examined the relationship between the SLP and mean ocean current (figure 4) during each period shown in figure 3(b). These years (1979–2018) are crudely split into three phases according to whether the temporal coefficient of the ocean current mode are dominated by positive or negative values (figure 3(b)); notably, the observed DSW salinity in TNBP develops in a similar temporal structure with 4 years lag (figure 2(a)) and can also be classified in the same phases according to the positive/negative salinity anomalies. The mean ocean circulation shows a cyclonic circulation at the surface in all phases (figures 4(a), (c) and (e)), representing the main current system in the RS, the Ross Gyre, which controls the cross shelf exchanges and westward transport from the upstream AS in the gyre's southern flank (Dotto *et al* 2018). Because zonal wind is found to be closely associated with changes of strength and location in the ASL (Paolo *et al* 2018, Raphael *et al* 2019), the wind-driven circulation in the RS is also expected to be affected by the ASL. Distinct spatial patterns of surface circulation are detected as a response to the SLP distribution driven by the ASL changes for different phases. In Phase I (1979–1986) and Phase III (2012–2018), although the center of the ASL displaces toward opposite directions, the region of low pressure extends consistently toward southwest relative to that in Phase II (red and black contour in figure 4, respectively). This increases the zonal gradient of the SLP between the Antarctica continental high and the ASL in Phase I and Phase III, driving the meridional flow at surface to become more dominant on the eastern RS shelf (figures 4(a) and (e)). As a result, the corresponding ocean current anomalies in Phases I and III exhibit a reversed orientation on the shelf (figures 4(b) and (f)). The decreased SLP is much more significant in Phase III (figure 4(e)), indicating an accelerated deepening of

the ASL after 2011 (figure 3(b)). This induces a strong eastward coastal current anomaly around the Antarctica (figure 4(f)), reduces the freshwater input to the RS from upstream regions, and results in a rapid increase of DSW salinity in recent years (figure 2(a)). In contrast, the slightly northeastward shift of the ASL (yellow contour in figure (4)) and positive SLP anomalies during Phase II (1987–2011, figures 4(c) and (d)) drive a westward anomaly of the coastal current, enhance the westward transport of freshwater from the AS and lead to the freshening trend before 2013. This suggests that the large-scale circulation changes are strongly modulated by the ASL, and the corresponding changes of westward transport of freshwater along the coastal current are responsible for the multidecadal variability in DSW salinity.

4. Conclusions

The production of DSW on the continental shelf of the RS contributes ~25% of the AABW to the global ocean (Orsi *et al* 2002). Hence, changes in DSW properties are expected to have global-scale impacts on heat exchanges through thermohaline circulation (Orsi and Wiederwohl 2009). Marked freshening of DSW has been detected and ascribed to increasing freshwater input resulting from the rapid melting of ice shelves in the upstream AS (Jacobs and Giulivi 2010, Budillon *et al* 2011). Using long-term records of observational temperature and salinity in the TNBP, we confirm recent studies showing a significant multidecadal variability of DSW salinity in the western RS. The freshening trend of DSW salinity before 2013 is estimated to be 0.052 ± 0.026 decade^{-1} (significant at 99% confidence level), and then is followed by an abrupt salinity enhancement thereafter. Earlier studies suggest that large-scale circulation changes and the resulting variability of freshwater input along coastal current from the AS to the RS are responsible for long-term changes of DSW salinity (Jacobs and Giulivi 2010, Castagno *et al* 2019). Based on the yearly mean ocean current derived from daily ice motion vectors and surface wind velocity, we find DSW salinity anomaly in TNBP is significantly correlated ($r = 0.72$, $p < 0.01$) with the zonal flow anomaly at the AS/RS gate with 4 years lag. With the mean absolute velocity along the coast from the AS/RS gate to the TNBP estimated to be 1.21 ± 0.24 cm s^{-1}, the low-salinity water parcels from upstream regions travel on average 1145 ± 227 km in 3 years after leaving the AS/RS gate along the coastal current, influencing DSW salinity of TNBP in summer months of the forth year.

The MCA results show that surface circulation controlling the westward transport on the southern flank of the Ross Gyre, i.e. the coastal current, is significantly coupled with SLP changes ($r = 0.53$ with $p < 0.01$), and both principal components are closely linked to the temporal evolution of the ASL. Spatial pattern variability of the circulation is largely modulated by the strength and shift of the ASL. In 1979–1986 and 2012–2018, the deepening of the ASL extends the region of low pressure toward southwest. This increases the zonal gradient of the SLP in the RS and makes the meridional flow become more dominant, resulting in an eastward coastal current anomaly on the shelf and a reduction in the freshwater input to the RS along the coastal current. By contrast, in 1987–2011, the northeastward shift of the ASL induces a westward coastal current anomaly, increases freshwater inflow to the RS and explains the long-term freshening before 2013. Given the connection constructed between multidecadal variability of the zonal flow and DSW salinity, it is reasonable to conclude that the deepening and southwestward extension of the ASL and the subsequent response of large-scale circulation determine the coastal current changes in upstream regions and the freshwater input to the RS, and are responsible for the multi-decadal variability of the DSW salinity in the western RS.

Data availability

Temperature and salinity records from the WOD13 datasets are available at https://www.nodc.noaa.gov/OC5/WOD13/, and records in and after 2013 are held by the Chinese National Arctic and Antarctic Data Center (http://www.chinare.org.cn). The ERA5 hourly data on single levels of SLP and wind velocity at 10 m are from https://doi.org/10.24381/cds.adbb2d47. The daily ice motion vectors are available at https://doi.org/10.5067/INAWUWO7QH7B. The ASL index is obtained from https://legacy.bas.acuk/dat a/absl/.

The data that support the findings of this study are available upon reasonable request from the authors.

Acknowledgments

This work was supported by the program of Response and Feedback of the Southern Ocean to Climate Change (Grant No. RFSOCC2020-2025), the Basic Scientific Fund for National Public Research Institutes of China (Grant No. 2018S02), the National Natural Science Foundation of China (Grant Nos. 41706220 and 41876231), and the National Key R&D Program of China (Grant Nos. 2018YFA0605701 and 2019YFC1509102). We are grateful to the staff of Chinese Arctic and Antarctic Administration and the crew of the R/V Xuelong for their professional supports in the Antarctic cruises. We thank Laurie Padman and an anonymous reviewer and the editor for their constructive feedback during the review process. We also want to give great thanks to many other individuals who contribute the in situ measurements and data processing over many years.

ORCID iDs

Guijun Guo https://orcid.org/0000-0002-1437-1561
Libao Gao https://orcid.org/0000-0002-0402-9340
Jiuxin Shi https://orcid.org/0000-0002-5825-8894

References

Adusumilli S, Fricker H A, Medley B, Padman L and Siegfried M R 2020 Interannual variations in meltwater input to the Southern Ocean from Antarctic ice shelves *Nat. Geosci.* **13** 616–20

Assmann K M and Timmermann R 2005 Variability of dense water formation in the Ross Sea *Ocean Dyn.* **55** 68–87

Böning C W, Dispert A, Visbeck M, Rintoul S R and Schwarzkopf F U 2008 The response of the Antarctic circumpolar current to recent climate change *Nat. Geosci.* **1** 864–9

Boyer T P *et al* 2013 World ocean database 2013 (Atlas) *Dataset* (https://doi.org/10.7289/V5NZ85MT)

Bretherton C S, Smith C and Wallace J M 1992 An intercomparison of methods for finding coupled patterns in climate data *J. Clim.* **5** 541–60

Budillon G, Castagno P, Aliani S, Spezie G and Padman L 2011 Thermohaline variability and Antarctic bottom water formation at the Ross Sea shelf break *Deep-Sea Res.* I **58** 1002–18

Budillon G, Pacciaroni M, Cozzi S, Rivaro P, Catalano G, Ianni C and Cantoni C 2003 An optimum multiparameter mixing analysis of the shelf waters in the Ross Sea *Antarct. Sci.* **15** 105–18

Castagno P, Capozzi V, Ditullio G R, Falco P, Fusco G, Rintoul S R, Spezie G and Budillon G 2019 Rebound of shelf water salinity in the Ross Sea *Nat. Commun.* **10** 5441

Castagno P, Falco P, Dinniman M S, Spezie G and Budillon G 2017 Temporal variability of the circumpolar deep water inflow onto the Ross Sea continental shelf *J. Mar. Syst.* **166** 37–49

Copernicus Climate Change Service (C3S) 2017 ERA5: fifth generation of ECMWF atmospheric reanalyses of the global climate *Dataset* (https://doi.org/10.24381/cds.adbb2d47)

Depoorter M A, Bamber J L, Griggs J A, Lenaerts J T, Ligtenberg S R, van den Broeke M R and Moholdt G 2013 Calving fluxes and basal melt rates of Antarctic ice shelves *Nature* **502** 89–92

Dinniman M S, Klinck J M and Hofmann E E 2012 Sensitivity of circumpolar deep water transport and ice shelf basal melt along the west Antarctic Peninsula to changes in the winds *J. Clim.* **25** 4799–816

Dinniman M S, Klinck J M, Hofmann E E and Smith W O 2018 Effects of projected changes in wind, atmospheric temperature, and freshwater inflow on the Ross Sea *J. Clim.* **31** 1619–35

Dotto T S, Naveira Garabato A, Bacon S, Tsamados M, Holland P R, Hooley J, Frajka-Williams E, Ridout A and Meredith M P 2018 Variability of the Ross Gyre, Southern Ocean: Drivers and responses revealed by satellite altimetry *Geophys. Res. Lett.* **45** 6195–204

Gao L, Rintoul S R and Yu W 2018 Recent wind-driven change in Subantarctic mode water and its impact on ocean heat storage *Nat. Clim. Change* **8** 58–63

Gille S T 2008 Decadal-scale temperature trends in the Southern Hemisphere Ocean *J. Clim.* **21** 4749–65

Gordon A L, Huber B A and Busecke J 2015 Bottom water export from the western Ross Sea, 2007 through 2010 *Geophys. Res. Lett.* **42** 5387–94

Gordon A L, Orsi A H, Muench R, Huber B A, Zambianchi E and Visbeck M 2009 Western Ross Sea continental slope gravity currents *Deep-Sea Res.* II **56** 796–817

Hosking J S, Orr A, Bracegirdle T J and Turner J 2016 Future circulation changes off West Antarctica: sensitivity of the Amundsen Sea low to projected anthropogenic forcing *Geophys. Res. Lett.* **43** 367–76

Hosking J S, Orr A, Marshall G J, Turner J and Phillips T 2013 The influence of the Amundsen–Bellingshausen Seas low on the climate of West Antarctica and its representation in coupled climate model simulations *J. Clim.* **26** 6633–48

Jacobs S S, Amos A F and Bruchhausen P M 1970 Ross sea oceanography and Antarctic bottom water formation *Deep-Sea Res.* **17** 935–62

Jacobs S S and Giulivi C F 2010 Large multidecadal salinity trends near the Pacific–Antarctic continental margin *J. Clim.* **23** 4508–24

Jacobs S S, Giulivi C F and Mele P A 2002 Freshening of the Ross Sea during the late 20th century *Science* **297** 386–9

Jendersie S, Williams M J M, Langhorne P J and Robertson R 2018 The density-driven winter intensification of the Ross Sea circulation *J. Geophys. Res.Oceans* **123** 7702–24

Johnson G C 2008 Quantifying Antarctic bottom water and North Atlantic deep water volumes *J. Geophys. Res.Oceans* **113** C05027

Kimura N 2004 Sea ice motion in response to surface wind and ocean current in the Southern Ocean *J. Meteorol. Soc. Japan* II **82** 1223–31

Kimura N and Wakatsuchi M 2000 Relationship between sea-ice motion and geostrophic wind in the northern hemisphere *Geophys. Res. Lett.* **27** 3735–8

Le Quéré C *et al* 2007 Saturation of the Southern Ocean CO_2 sink due to recent climate change *Science* **316** 1735–8

Lumpkin R and Speer K 2007 Global ocean meridional overturning *J. Phys. Oceanogr.* **37** 2550–62

Marshall J and Speer K 2012 Closure of the meridional overturning circulation through Southern Ocean upwelling *Nat. Geosci.* **5** 171–80

Meredith M P, Naveira Garabato A C, Hogg A M and Farneti R 2012 Sensitivity of the overturning circulation in the Southern Ocean to decadal changes in wind forcing *J. Clim.* **25** 99–110

Nakayama Y, Timmermann R, Rodehacke C B, Schröder M and Hellmer H H 2014 Modeling the spreading of glacial meltwater from the Amundsen and Bellingshausen Seas *Geophys. Res. Lett.* **41** 7942–9

Nihashi S and Ohshima K I 2015 Circumpolar mapping of Antarctic coastal polynyas and landfast sea ice: relationship and variability *J. Clim.* **28** 3650–70

Orsi A H, Johnson G C and Bullister J L 1999 Circulation, mixing, and production of Antarctic bottom water *Prog. Oceanogr.* **43** 55–109

Orsi A H, Smethie W M Jr and Bullister J L 2002 On the total input of Antarctic waters to the deep ocean: a preliminary estimate from chlorofluorocarbon measurements *J. Geophys. Res.Oceans* **107** 31–1–31–14

Orsi A H and Wiederwohl C L 2009 A recount of Ross Sea waters *Deep-Sea Res.* II **56** 778–95

Paolo F S, Fricker H A and Padman L 2015 Volume loss from Antarctic ice shelves is accelerating *Science* **348** 327–31

Paolo F S, Padman L, Fricker H A, Adusumilli S, Howard S and Siegfried M R 2018 Response of Pacific-sector Antarctic ice shelves to the El Nino/Southern Oscillation *Nat. Geosci.* **11** 121–6

Pritchard H D, Ligtenberg S R, Fricker H A, Vaughan D G, van den Broeke M R and Padman L 2012 Antarctic ice-sheet loss driven by basal melting of ice shelves *Nature* **484** 502–5

Raphael M N, Holland M M, Landrum L and Hobbs W R 2019 Links between the Amundsen Sea Low and sea ice in the Ross Sea: seasonal and interannual relationships *Clim. Dyn.* **52** 2333–49

Rignot E, Jacobs S, Mouginot J and Scheuchl B 2013 Ice-shelf melting around Antarctica *Science* **341** 266–70

Rignot E, Mouginot J, Scheuchl B, van den Broeke M, van Wessem M J and Morlighem M 2019 Four decades of Antarctic Ice Sheet mass balance from 1979–2017 *Proc. Natl Acad. Sci.* **116** 1095–103

Rintoul S R, Silvano A, Pena-Molino B, van Wijk E, Rosenberg M, Greenbaum J S and Blankenship D D 2016 Ocean heat drives rapid basal melt of the Totten Ice Shelf *Sci. Adv.* **2** e1601610

Roquet F *et al* 2014 A Southern Indian Ocean database of hydrographic profiles obtained with instrumented elephant seals *Sci. Data* **1** 140028

Rusciano E, Budillon G, Fusco G and Spezie G 2013 Evidence of atmosphere–sea ice–ocean coupling in the Terra Nova Bay polynya (Ross Sea–Antarctica) *Cont. Shelf Res.* **61–62** 112–24

Shepherd A *et al* 2018 Mass balance of the Antarctic Ice Sheet from 1992 to 2017 *Nature* **558** 219–22

Smith W O, Dinniman M S, Hofmann E E and Klinck J M 2014 The effects of changing winds and temperatures on the oceanography of the Ross Sea in the 21st century *Geophys. Res. Lett.* **41** 1624–31

Spence P, Griffies S M, England M H, Hogg A M, Saenko O A and Jourdain N C 2014 Rapid subsurface warming and circulation changes of Antarctic coastal waters by poleward shifting winds *Geophys. Res. Lett.* **41** 4601–10

Steele M, Zhang J, Rothrock D and Stern H 1997 The force balance of sea ice in a numerical model of the Arctic Ocean *J. Geophys. Res.Oceans* **102** 21061–79

Tamura T, Ohshima K I, Fraser A D and Williams G D 2016 Sea ice production variability in Antarctic coastal polynyas *J. Geophys. Res.Oceans* **121** 2967–79

Thoma M, Jenkins A, Holland D and Jacobs S 2008 Modelling Circumpolar Deep Water intrusions on the Amundsen Sea continental shelf, Antarctica *Geophys. Res. Lett.* **35** L18602

Thorndike A S and Colony R 1982 Sea ice motion in response to geostrophic winds *J. Geophys. Res.Oceans* **87** 5845–52

Tschudi M, Meier W N, Stewart J S, Fowler C and Maslanik J 2019 Polar pathfinder daily 25 km EASE-grid sea ice motion vectors, version 4 from NASA National Snow and Ice Data Center Distributed Active Archive Center *Dataset* (https://doi.org/10.5067/INAWUWO7QH7B)

Turner J, Orr A, Gudmundsson G H, Jenkins A, Bingham R G, Hillenbrand C-D and Bracegirdle T J 2017 Atmosphere-ocean-ice interactions in the Amundsen Sea Embayment, West Antarctica *Rev. Geophys.* **55** 235–76

Turner J, Phillips T, Hosking J S, Marshall G J and Orr A 2013 The Amundsen Sea low *Int. J. Climatol.* **33** 1818–29

Wallace J M, Smith C and Bretherton C S 1992 Singular value decomposition of wintertime sea surface temperature and 500-mb height anomalies *J. Clim.* **5** 561–76

Williams G D *et al* 2016 The suppression of Antarctic bottom water formation by melting ice shelves in Prydz Bay *Nat. Commun.* **7** 12577